TOXICOLOGICAL SCIENCES **130(1)**, 145–157 (2012)
doi:10.1093/toxsci/kfs225
Advance Access publication July 24, 2012

Global Gene Expression Profiling of Human Lung Epithelial Cells After Exposure to Nanosilver

Rasmus Foldbjerg,* Eveline S. Irving,* Yuya Hayashi,† Duncan S. Sutherland,† Kasper Thorsen,‡ Herman Autrup,* and Christiane Beer*,[1]

*Department of Public Health, Aarhus University, DK-8000 Aarhus C, Denmark; †Interdisciplinary Nanoscience Center, Aarhus University, DK-8000 Aarhus C, Denmark; and ‡Department of Molecular Medicine, Aarhus University Hospital, DK-8200 Aarhus N, Denmark

[1]To whom correspondence should be addressed at Department of Public Health, Aarhus University, Bartholins Allé 2, 8000 Aarhus C, Denmark. Fax: +45 8942 6200. E-mail: cbee@mil.au.dk.

Received March 19, 2012; accepted July 12, 2012

The toxic effects of silver nanoparticles (AgNPs) on cells are well established, but only limited studies on the effect of AgNPs and silver ions on the cellular transcriptome have been performed. In this study, the effect of AgNPs on the gene expression in the human lung epithelial cell line A549 exposed to 12.1 µg/ml AgNPs (EC20) for 24 and 48 h was compared with the response to control and silver ion (Ag^+) treated cells (1.3 µg/ml) using microarray analysis. Twenty-four hours to AgNP altered the regulation of more than 1000 genes (more than twofold regulation), whereas considerably fewer genes responded to Ag^+ (133 genes). The upregulated genes included members of the metallothionein, heat shock protein, and histone families. As expected from the induction of metallothionein and heat shock protein genes, Ag^+ and AgNP treatment resulted in intracellular production of reactive oxygen species but did not induce apoptosis or necrosis at the concentrations used in this study. In addition, the exposure to AgNPs influenced the cell cycle and led to an arrest in the G2/M phase as shown by cell cycle studies by flow cytometry and microscopy. In conclusion, although the transcriptional response to Ag^+ exposure was highly related to the response caused by AgNPs, our findings suggest that AgNPs, due to their particulate form, affect exposed cells in a more complex way.

Key Words: **Nanotoxicology; silver nanoparticles; gene expression; stress; cell cycle.**

Nanoparticles (NPs) are increasingly used in consumer products and therefore knowledge on their biological effects is of outermost importance. Silver NPs (AgNPs) are among the most widely used NPs in consumer products and are used in bandages, textiles, and house-hold items exploiting the antimicrobial properties of silver (Marambio-Jones and Hoek, 2010; The Woodrow Wilson International Center, 2011). Although of known chemical composition, their small size with at least one dimension between 1 and 100 nm leads to advanced chemical and physical characteristics compared with the bulk counterpart. Especially, the higher surface to volume ratio of NPs is a cause for concern as it makes NPs not only potentially more reactive than larger particles but makes it more difficult to predict the way NPs interact with biological systems (Landsiedel *et al.*, 2010; Maynard *et al.*, 2011; Oberdörster *et al.*, 2005). Exposure to metallic silver is generally considered to pose minimal health risks although intake of colloidal and soluble silver at high concentrations can cause argyria, an irreversible deposition of silver in the skin. Besides argyria, exposure to soluble silver compounds may induce other toxic effects, including liver and kidney damage, irritation of the eyes, skin, respiratory, and intestinal tract, and changes in hematological parameters (Drake and Hazelwood, 2005). Both *in vitro* and *in vivo* studies have demonstrated toxic effects of AgNPs (Foldbjerg *et al.*, 2011, 2009; Kawata *et al.*, 2009), and recently we reported that free silver ions (Ag^+) play a major part in the toxicity of AgNPs due to a high initial Ag^+ content present in the AgNP suspension (Beer *et al.*, 2012). However, it is not clear whether the mechanism of action for AgNP toxicity is related to the nanosize, the amount of silver ions, or whether it is a combination of both. Many other NP parameters determine the toxicity of NPs, e.g., size and shape (Hsiao and Huang, 2011; Karlsson *et al.*, 2009; Napierska *et al.*, 2009; Yamamoto *et al.*, 2004). To explore and compare the mechanisms behind AgNP and Ag^+ induced toxicity, we performed global gene expression analysis in A549 human lung epithelial cells and related these results to investigations of the cell cycle, apoptosis, and induction of reactive oxygen species (ROS).

MATERIALS AND METHODS

Materials and reagents. $AgNO_3$ (Reag. Ph. Eur.) was obtained from Sigma Aldrich (no. 35375). Dulbecco's modified Eagle's medium (DMEM) (no. 61965), heat-inactivated fetal bovine serum (FBS) (Gibco, no. 10500-064), L-alanyl-L-glutamine, annexin V-Alexa Fluor 488, propidium iodide (PI), penicillin, and streptomycin were purchased from Invitrogen.

HNO_3 (69%), 2′,7′-dichlorodihydrofluorescein diacetate (H_2DCF-DA), 3-(4,5-dimethyl-2-thiazolyl)-2,5-diphenyl-2H-tetrazolium bromide (MTT), and dimethylsulfoxide were purchased from Sigma Aldrich. NIM-DAPI was purchased from Beckman Coulter; RNeasy was purchased from Qiagen.

Laboratory synthesis of colloidal AgNPs. Colloidal AgNPs were synthesized by chemical reduction of the silver salt in sodium citrate as described previously (Beer *et al*., 2012). Briefly, solutions of silver nitrate ($AgNO_3$) and sodium citrate tribasic dihydrate were mixed, to which sodium borohydride ($NaBH_4$) solution was added in one batch while stirring vigorously at room temperature (RT). The solution temperature was gradually raised to 70°C and heated further. After cooling to RT, bovine serum albumin (BSA) solution was injected to facilitate steric stabilization of the colloidal system. A diafiltration kit (Amicon Ultra centrifugal filter units, 100 kDa cutoff regenerated cellulose membrane; Millipore) was used to remove residual reactants and BSA. The total silver concentration was determined by flame atomic absorption spectrophotometry (see below), and the stock solution was stored at 4°C in the dark until use. The concentrations of total silver in the AgNP stock suspension and its supernatant were determined by atomic absorption spectrophotometry after acid digestion as described previously (Beer *et al*., 2012).

Calculation of final silver ion concentration. In this study, $AgNO_3$ was used as control for the Ag^+ fraction present in the AgNP suspension. As AgNPs release Ag^+ over time, the maximal concentration of released Ag^+ was calculated based on the publication of Kittler *et al*. (2010) in which the Ag^+ release kinetic is described by a modified first-order reaction kinetic rate equation $y(t) = y(\text{final})(1–\exp(–kt))$, with $y(t)$ is the released amount of Ag^+ in %, y(final) is the maximal percentage of released Ag^+, k is a rate coefficient, and t is the time in hours. Kittler *et al.* calculated values for y(final) = 56% and $k = 0.0023\,h^{-1}$ for citrate-stabilized AgNPs at 37°C. Using these values, we calculated the amount of released Ag^+ after 48-h incubation to be 3.85% of the original AgNP concentration. The final used Ag^+ concentration was calculated to 1.3 µg/ml (0.6 µg/ml initial Ag^+ fraction plus 0.7 µg/ml maximal released Ag^+ after 48 h).

Particle characterization. Technical details of primary and *in situ* characterization methods for AgNPs are described in our previous publications (Beer *et al*., 2012; Foldbjerg *et al*., 2009). Briefly, distribution of primary particle sizes was established using transmission electron microscopy followed by image analysis of size statistics. The homogeneity of particle sizes and shapes was optically studied by inspecting the surface plasmon resonance of colloidal AgNPs analyzed as absorbance spectra scanned on a UV-visible spectrophotometer (UV-vis). Zeta potential of AgNPs (in MilliQ water) was measured at 25°C using a Malvern's zetasizer device. Dynamic light scattering (DLS) was used to estimate the hydrodynamic size and colloidal stability of AgNPs at ionic strength of 10mM (NaCl solution, as reference) and in cell culture media (described below) with or without 2.5% heat-inactivated FBS. DLS analysis was performed in triplicate at 37°C after 24-h incubation under the culturing condition (37°C, 5% CO_2).

Cell culture. The A549 human lung carcinoma epithelial-like cell line was obtained from ATCC (no. CCL-185). Cells were cultured in DMEM supplemented with penicillin (100 µg/ml), streptomycin (100 U/ml), and 10% heat-inactivated FBS. Cells were maintained in a humidified atmosphere at 37°C and 5% CO_2.

For exposure studies with AgNP suspension, A549 cells were seeded in culture dishes and cultured in DMEM/10% FBS for 1 day prior to the exposure. For the exposure studies, AgNP stock suspension was diluted in DMEM/2.5% FBS. For the control, cell culture medium was diluted with water.

MTT assay. To measure the cellular mitochondrial activity, MTT assays were employed as previously described (Beer *et al*., 2012) with the modification that the A549 cells were seeded at 1×10^4 cells per well and incubated in DMEM/2.5% FBS with or without AgNPs for 24 h at 37°C, 5% CO_2.

AgNP exposure, gene array hybridization, and data analysis. A549 cells were seeded (5×10^5 cells in a 75-cm^2 cell culture flask) to ensure a cell density of approximately 80% confluence at the end of the exposure time. On the following day, cells were treated with 12.1 µg/ml laboratory-synthesized AgNPs for 24 or 48 h. This concentration corresponded to a 20% decrease in metabolic activity (EC20) after 24 h based on data from MTT assays (supplementary data). Sterile ddH2O was added as vehicle control. Using the same procedure, A549 cells were treated with 1.3 µg/ml Ag^+, which corresponds to the amount of the initial silver ion fraction plus the calculated maximal amount of Ag^+ resulting from the dissolution of the AgNPs during the incubation period (see Calculation of Used Silver Ion Concentration). For use in microarray analysis, total RNA was isolated after 24 and 48 h of exposure using Qiagen RNeasy mini kit as described by the manufacturer.

The Ambion WT Expression Kit (Ambion) was used to label 100 ng total RNA according to the manufacturer's instructions and was hybridized overnight to the GeneChip Human Gene 1.0 ST Arrays (Affymetrix). Quality control was performed in the Expression Console software (Affymetrix) where control probe sets along with labeling and hybridization control in data were interrogated. Furthermore, to evaluate the biological similarity of all samples, principal component analysis and hierarchical clustering (using Euclidian distance and centroid linkage) were performed. Data were quantile normalized in the GeneSpring GX 11.5 software (Agilent) using the iterPL IER16 algorithm. Fold change differences were calculated for all pairs of samples, and only genes exhibiting at least a twofold expression difference in all pairs of samples were considered to be differentially expressed and subsequently used for pathway analysis in the Ingenuity pathway analysis software (Ingenuity Systems) and the Database for Annotation, Visualization, and Integrated Discovery (DAVID), where default settings in the functional annotation tool were used (Huang *et al*., 2009a,b). Hierarchical clustering was performed using Euclidian distance and centroid linkage. The raw data and Robust Multi-array Average (RMA) normalized data of the microarrays are available via MIAMExpress (http://www.ebi.ac.uk/miamexpress/), accession number E-MEXP-3583.

RT-qPCR and data analysis. To validate microarray gene expression data, A549 cells were seeded with 2.5×10^5 cells per 60-mm dish and grown to 80% density before treated with Ag^+ or AgNPs for 24 h. Sterile ddH2O was added as vehicle control. Total RNA was isolated after 24 h of exposure using Qiagen RNeasy mini kit as described by the manufacturer. cDNA was synthesized from 1 µg total RNA using the QuantiTect Reverse Transcription Kit (Qiagen) as described by the manufacturer. qPCR was performed using the QuantiTect SYBR Green Kit + UNG treatment (Qiagen) and QuantiTect Primer (Qiagen) for human *HIST1H1B*, *CCNB1*, and *MT1B* genes on an ABI Prism 7000 Sequence Detection System (Applied Biosystems) with the following qPCR program: 2 min, 50°C (UNG reaction); 15 min, 95°C; 40 cycles, 15 s, 94°C; 30 s, 55°C; and 30 s, 72°C. In each qPCR run as control, H_2O was added to the qPCR reaction instead of cDNA, which in all cases was negative (data not shown). The specificity of the reaction was confirmed by melting curves and DNA agarose gels (data not shown). Raw data from three experiments (biological replicates) performed in triplicates were analyzed using the standard setting of the DART PCR program version 1.0 (Peirson *et al*., 2003) to calculate the C_t value and the efficiency of the qPCR reaction. Ratios of the samples compared with control were calculated using the formula: Ratio = $(\text{Efficiency}_{\text{target}})^{\Delta C_t\,(\text{control-sample})}$ (Pfaffl, 2001). As the treatment with Ag NPs had a profound effect on the gene expression, the Norma-Gene program was used for normalization of the qPCR data using the standard settings (Heckmann *et al*., 2011).

Cell cycle synchronization and cell cycle analysis. To study the effect of AgNPs on the cell cycle, cells were synchronized by washing twice with serum-free cell culture medium followed by culturing in serum-free cell culture medium for 3 days. After 3 days, the cells were exposed to Ag^+, AgNPs, or water as control in cell culture medium containing 2.5% FBS. After 24-h or 48-h exposure, cell cycle analyses were performed using NIM-DAPI (Beckman Coulter). The cells were pelleted after exposure at 300 × g and resuspended in PBS. Subsequently, an equal volume of NIM-DAPI solution was added to the cells and kept on ice until analyzed in a flow cytometer (Cell Lab Quanta SCMPL, Beckman Coulter). The UV arc lamp with a 355/37BP filter was used

for excitation, and fluorescence was detected in FL-1 using 465/30BP filter. For each sample, 1 to 2×10^4 cells were investigated.

For microscopic investigations, synchronized cells were seeded at 1×10^4 cells per well of an eight-well chamber slide, fixed with 4% paraformaldehyde, washed thrice with PBS, and covered using DAPI containing VectaShield mounting medium. Pictures were taken at 200× magnification using a DAPI filter.

ROS assay. The intracellular generation of ROS was measured by using the fluorescent marker H_2DCF-DA as previously described by Krejsa and Schieven (2000) with minor modifications. The cells were incubated with 5µM 2,7-dichlorodihydrofluorescein (DCF) diacetate in PBS for 20 min, subsequently washed with PBS, and resuspended at the desired concentration in phenol red–free DMEM medium with 2.5% FBS. Cells were exposed to AgNPs and Ag^+ in six-well plates, and after 24 h, the cells were detached from the culture plates and 300 µl cell suspensions were transferred to sample cups and immediately analyzed by flow cytometry (Cell Lab Quanta SCMPL, Beckman Coulter). A 488-nm wavelength laser was used for excitation, and fluorescence was detected in FL-1 using a 525/30 BP filter. The mean fluorescence of 2×10^4 cells was determined for each sample by FlowJo software ver. 7.6.4 (Tree Star, Inc.).

Annexin V/PI assay. The ratio of apoptotic and necrotic cells was measured with the annexin V/PI assay (van Engeland *et al.*, 1996). After NP exposure, cells were trypsinized and washed in PBS and subsequently in binding buffer (10mM HEPES, pH 7.4; 140mM NaCl; 2.5mM $CaCl_2$). Staining was performed in the dark for 10 min at RT in 100 µl binding buffer containing annexin V-Alexa 488 (40 µl/ml) and PI (1 µg/ml). Finally, 400 µl binding buffer was added to each sample, and cells were kept on ice and analyzed by flow cytometry within 1 h. The 488-nm wavelength laser was used for excitation, and Alexa 488 was detected in FL-1 using a 525/30 BP filter, whereas PI was detected in FL-2 using a 575/30 BP filter. Using single-stained and unstained cells, standard compensation was done in the Quanta SC MPL Analysis software (Beckman Coulter). For each sample, 2×10^4 cells were analyzed and early apoptotic (annexin V^+, PI^-), late apoptotic/necrotic (annexin V^+, PI^+), and live (annexin V^-, PI^-) cells were expressed as percentages of the measured 2×10^4 cells using the FlowJo software ver. 7.6.4 (Tree Star, Inc.).

Statistical analysis. Data are expressed as mean ± SD. The statistical significance was determined by Student's *t*-test ($p < 0.05$) assuming normally distributed sample data and equal variances. For analysis of enriched gene ontology (GO) terms, the integrated statistical analysis of DAVID was used and GO terms with false discovery rate (FDR) adjusted *p* value > 0.05 were disregarded. Normalized qPCR gene expression data were analyzed by one way ANOVA followed by Tukey's test. Before analysis, data were log-transformed to obtain equal variances (Bartlett's test), and normality was assumed. Statistical analysis was performed in Stata/IC ver. 11.2 and SigmaPlot ver. 11.

RESULTS

Silver Nanoparticle Characterization

A summary of the physicochemical characterization of AgNPs is given in Table 1. Laboratory synthesis of AgNPs yielded spherical particles (aspect ratio = 1.1 ± 0.1, SD, $n = 490$) with a mean size of 15.9 ± 7.6 nm (SD, $n = 490$) (Fig. 1A). Gaussian fitting of the size frequencies shows a skewed, log-normal distribution with a tail toward larger diameters (Fig. 1A, inset). Colloidal homogeneity was reflected in the surface plasmon resonance with a characteristic peak at 420 nm (Fig. 1B). In contrast, DLS analysis showed a bimodal distribution of the hydrodynamic size under all conditions tested (Fig. 1C). BSA pretreatment of (citrate-capped) AgNPs successfully facilitated spontaneous formation of NP-protein corona establishing steric mechanisms and thus preventing particle aggregation at high ionic strength (cf. "in 10mM NaCl" compared with "in DMEM, 24 h" in Fig. 1C). Addition of serum (2.5% FBS) shifted the size peak toward slightly larger particle sizes after 24-h incubation (Fig. 1C), a result of protein exchange overwriting the corona profile. Such size shifts are also apparent in the primary peak below 10 nm, reflecting the differential distribution of free proteins (or protein aggregates). The initial silver ion fraction of the AgNP solution was maximal 4.99% as measured by AAS after removal of the major part of the AgNPs by ultracentrifugation (Beer *et al.*, 2012).

Gene Expression Profiling

The changes in gene expression of A549 human lung epithelial cells in response to 24-h and 48-h exposure to AgNPs were investigated using Affymetrix microarrays. The cells were treated with 12.1 µg/ml AgNPs for 24 or 48 h (EC20). At this concentration, 80% of the cells were viable after 24 h as measured by MTT assay (Supplementary fig. S1A). In addition, only a slight increase of apoptotic and necrotic cells was detected by the annexin V/PI assay after 24 and 48 h of treatment at this concentration (Supplementary fig. S1B and S1C). To study the effect of Ag^+, A549 cells were treated with 1.3 µg/ml Ag^+, which corresponds to the amount of the initial Ag^+

TABLE 1
Characterization of Laboratory-Synthesized AgNPs

AAS	TEM			LDV*	DLS**	
Ag^+ fraction	Particle size	Particle aspect ratio	Calculated specific surface area	Zeta potential	Hydrodynamic size	PdI
4.99%	15.9 ± 7.6 nm SD ($n = 490$)	1.10 ± 0. 1 SD ($n = 490$)	24.5 m^2/g	−21.6 ± 1.3 mV SD ($n = 3$)	38.7 ± 23.0 nm Z-average ± PdI width	0.353

Note. TEM, transmission electron microscopy.
* Laser Doppler velocimetry.
** Values from measurements after 24-h incubation of AgNPs in DMEM/2.5% FBS under the culturing condition.

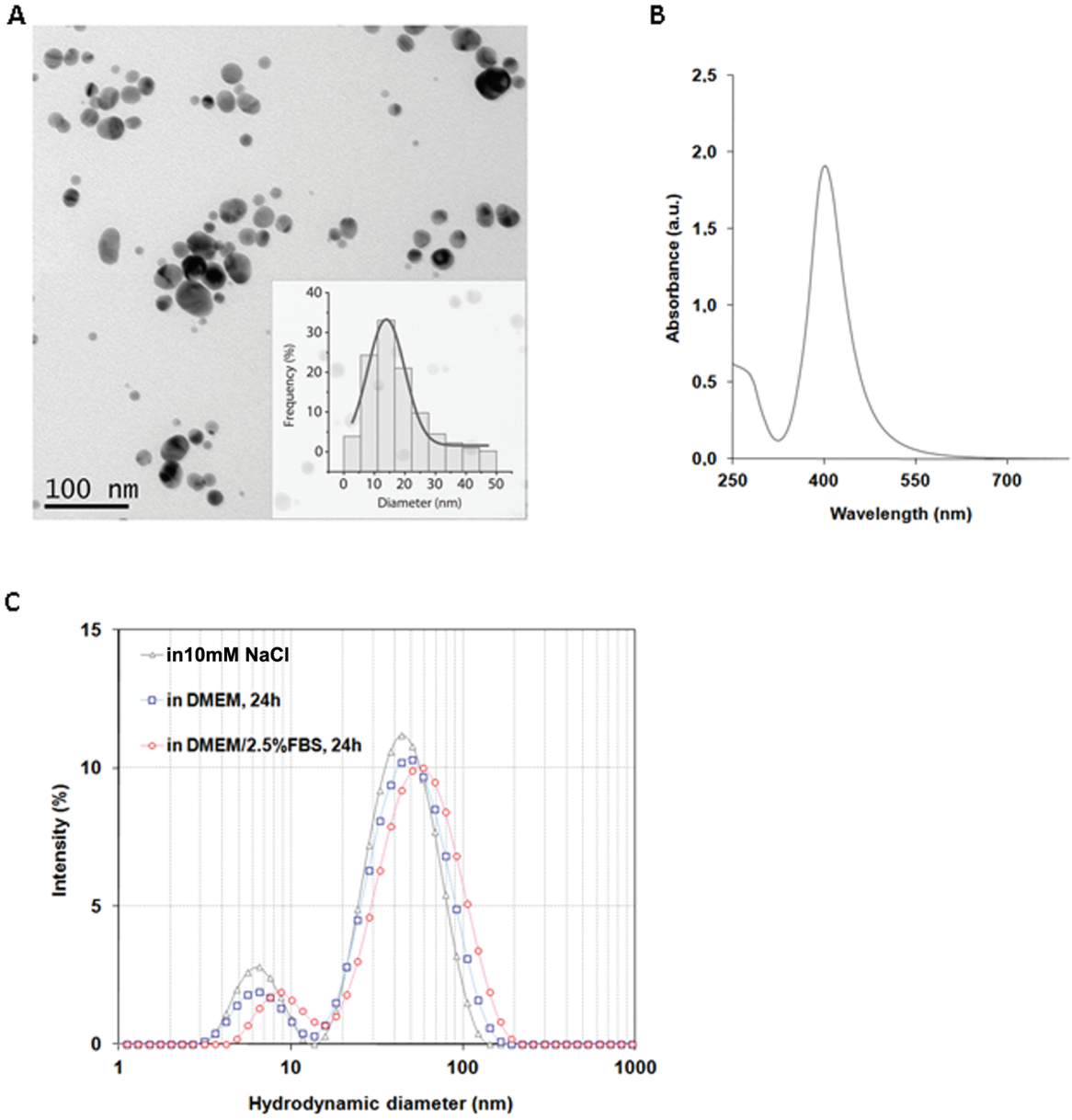

FIG. 1. Characterization of the laboratory-synthesized AgNPs. (A) TEM imaging of the AgNPs. The primary size distribution is shown in the inset. (B) UV-Vis spectrum displaying nanosilver-specific surface plasmon resonance. (C) Hydrodynamic size distribution of AgNPs in DMEM cell culture medium with or without FBS.

fraction plus the calculated maximal amount of Ag^+ resulting from the dissolution of the AgNPs during the incubation period. Principal component analysis of the microarray data showed that the pairs of the biological replicates of each exposure type (control, Ag^+, and AgNP) clustered together except for the replicates of the 48-h control (Fig. 2A). Because of the divergence between the two 48-h control replicates, they were excluded from further analysis. Hierarchical clustering analysis indicated that samples treated for 24 h with Ag^+ or AgNP were more related to each other than to the control. However, after 48-h exposure, Ag^+-treated cells exhibited a gene expression pattern, which was more related to that of control cells than to that of AgNP-treated cells (Fig. 2B).

The number of affected genes was considerably higher in the AgNP-treated cells than in Ag^+-treated cells. After 24-h exposure to AgNPs, 1013 genes were at least twofold up- or downregulated in all pairs of samples, whereas only 133 genes in Ag^+-treated cells were twofold regulated (Table 2). Compared with the controls, Ag^+ treatment mostly upregulated the genes (107 genes out of 133), whereas a smaller fraction were upregulated when cells were treated with AgNPs (538 upregulated genes vs. 475 downregulated genes). However,

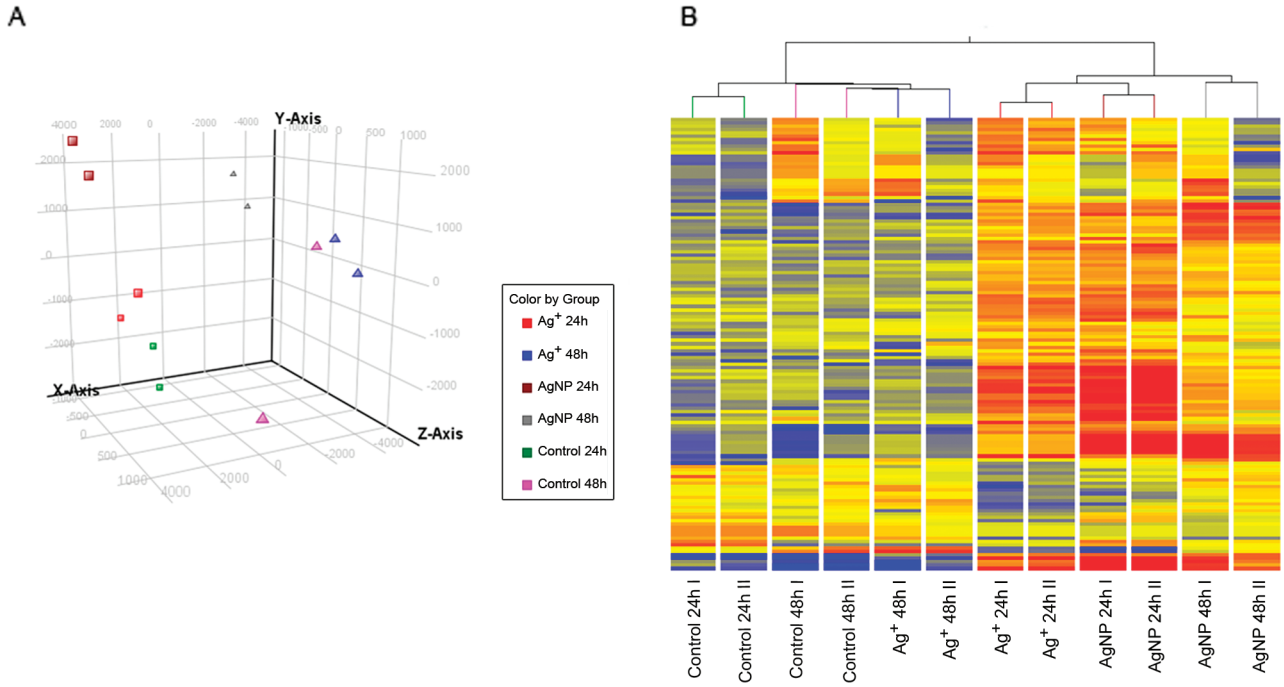

FIG. 2. (A) Principal component analysis. (B) Hierarchical clustering and heat map of the microarray experiment. Blue color indicates low expression levels, whereas red indicates high expression levels.

TABLE 2
Number of Genes That Were At Least Twofold Regulated in All Pairs of Samples in Response to 24-h Exposure With 1.3 µg/ml Ag^+ or 12.1 µg/ml AgNP

	Ag^+/Control	AgNP/Control	AgNP/Ag^+
All	133	1013	211
Upregulated	107	538	109
Downregulated	26	475	102

when directly comparing the gene expression of Ag^+-treated cells with AgNP-treated cells, the number of up- or downregulated genes was nearly the same (109 upregulated genes vs. 102 downregulated genes). Out of the 107 upregulated genes after Ag^+ treatment, 74 genes (60 plus 14, Fig. 3A) were also found to be regulated as response to AgNP treatment, whereas only 8 genes were downregulated in both Ag^+-treated cells and AgNP-treated cells (Fig. 3B). This suggests similarities in the reaction of the cells to Ag^+ and AgNP but that there are also fundamental differences. This could also be noticed when the data sets of the regulated genes were analyzed for functional annotations and their clustering in functional pathways using the DAVID (Huang *et al.*, 2009a,b). The most prominent GO terms significantly enriched in upregulated genes upon 24-h exposure, irrespective of whether present as Ag^+ or AgNPs, include genes from the metallothionein superfamily (Table 3A and B). In addition, in cells treated with Ag^+, GO terms such as copper ion binding, cadmium ion binding, and metal binding were present (Table 3B). When comparing the gene expression of AgNP with Ag^+-treated cells, eight GO terms were significantly enriched that mainly involved genes of stress response and response to unfolded proteins (Table 3C). For downregulated genes, significantly enriched GO terms were identified in the case of AgNP exposure (Table 4) and these genes were mostly involved in the regulation and execution of the cell cycle.

Cell Cycle Analysis and Gene Expression

An overview of the cell cycle pathway and the genes at least twofold regulated in all pairs of samples upon 24 h of exposure to Ag^+ or AgNP are shown in Figure 4. Several key genes of this pathway, like *cyclin B1*, *cyclin A*, *cdk1*, were downregulated by AgNP treatment, whereas genes like *GADD45* were upregulated. The downregulation of *cyclin B1* (*CCNB1*) and *histone H1.5* (*HIST1H1B*) for AgNP-treated cells was confirmed by RT-qPCR (Figs. 5E and F). In accordance with these findings, a number of histone genes were downregulated as a response to AgNP treatment whereas treatment with Ag^+ had nearly no effect on the expression of histone genes (Supplementary table 1). This was also confirmed by RT-qPCR, where Ag+ treatment had no effect on the expression of *HIST1H1B*. However, the same amount of silver added as AgNPs significantly downregulated *CCNB1* and *HIST1H1B* (Figs. 5E and F). The downregulated genes involve several genes coding for histone 1, 2, 3, and 4 proteins. After 48-h AgNP treatment, a profound upregulation of genes involved in the maintenance and execution of the

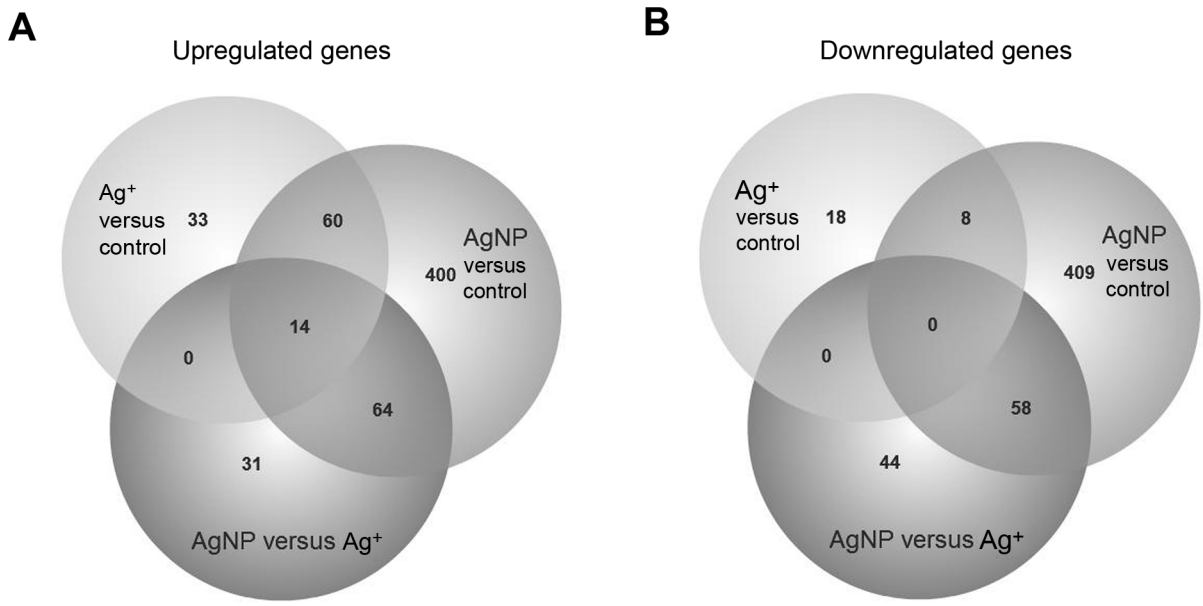

FIG. 3. Venn diagram of the regulated genes after 24 h of exposure with Ag^+ and AgNP in comparison to control or in comparison to each other. (A) Upregulated genes. (B) Downregulated genes.

TABLE 3
Functional Annotations Analysis of Microarray Data Sets Using DAVID (Huang *et al.*, 2009a,b)

Category	Term	Count	Fold enrichment	FDR*
(A) GO terms significantly enriched in genes at least twofold upregulated in response to Ag^+ exposure				
Interpro	Metallothionein, vertebrate	6	176.7	1.2E−7
Interpro	Metallothionein superfamily, eukaryotic	6	176.7	1.2E−7
SP_PIR_Keywords	Metal-thiolate cluster	6	176.2	1.2E−7
Interpro	Metallothionein, vertebrate, metal binding site	5	160.7	1.9E−5
UP_SEQ_Feature	Metal ion-binding site: Divalent metal cation; cluster A	5	162.7	2.0E−5
UP_SEQ_Feature	Metal ion-binding site: Divalent metal cation; cluster B	5	162.7	2.0E−5
PIR_Superfamily	Metallothionein	5	122.2	3.5E−5
SP_PIR_Keywords	Chelation	4	176.2	1.3E−3
SP_PIR_Keywords	Cadmium	4	176.2	1.3E−3
GOTerm_MF_FAT	Copper ion binding	6	29.2	1.8E−3
GOTerm_MF_FAT	Cadmium ion binding	4	130.3	3.5E−3
SP_PIR_Keywords	Copper	5	30.9	2.2E-2
SP_PIR_Keywords	Metal binding	4	74.2	2.2E−2
(B) GO terms significantly enriched in genes at least twofold upregulated in response to AgNP exposure				
SP_PIR_Keywords	Metal-thiolate cluster	7	29.6	6.3E−5
Interpro	Metallothionein superfamily, eukaryotic	7	29.9	6.4E−5
Interpro	Metallothionein, vertebrate	7	29.9	6.4E−5
Interpro	Metallothionein, vertebrate, metal binding site	6	28.0	1.7E−3
UP_SEQ_Feature	Metal ion-binding site: Divalent metal cation; cluster A	6	27.8	1.9E−3
UP_SEQ_Feature	Metal ion-binding site: Divalent metal cation; cluster B	6	27.8	1.9E−3
(C) GO terms significantly enriched in genes at least twofold upregulated when comparing exposure to AgNP and Ag^+				
SP_PIR_Keywords	Stress response	7	34.6	5.2E−5
GOTerm_BP_FAT	Response to protein stimulus	8	22.5	6.8E−5
GOTerm_BP_FAT	Response to unfolded protein	6	25.5	4.6E−3
Interpro	Heat shock protein Hsp70	4	112.9	5.8E−3
Interpro	Heat shock protein 70	4	112.9	5.8E−3
Interpro	Heat shock protein 70, conserved site	4	90.3	1.2E−2
GOTerm_BP_FAT	Response to organic substance	12	5.0	1.9E−2
KEGG_Pathway	MAPK signaling pathway	8	7.7	2.7E−2

Note. MAPK, mitogen-activated protein kinase.
*FDR, false discovery rate adjusted *p* value.

TABLE 4
Functional Annotations Analysis of Microarray Data Sets Using DAVID (Huang *et al.*, 2009a,b). GO Terms Significantly Enriched in Genes At Least Twofold Downregulated in Response to AgNP Exposure

Category	Term	Count	Fold enrichment	FDR*
GOTerm_BP_FAT	Cell cycle process	41	3.3	6.9E–8
GOTerm_BP_FAT	Cell cycle	49	2.9	7.1E–8
SP_PIR_Keywords	Cell cycle	36	3.5	5.0E–7
GOTerm_BP_FAT	Cell cycle phase	33	3.6	7.8E–7
GOTerm_BP_FAT	Mitosis	24	5.0	8.3E–7
GOTerm_BP_FAT	Nuclear division	24	5.0	8.3E–7
GOTerm_BP_FAT	M phase of mitotic cell cycle	24	4.9	1.1E–6
GOTerm_BP_FAT	Organelle fission	24	4.8	1.9E–6
GOTerm_BP_FAT	Mitotic cell cycle	30	3.7	4.1E–6
GOTerm_BP_FAT	M phase	28	3.9	5.2E–6
SP_PIR_Keywords	Mitosis	21	5.1	8.6E–6
SP_PIR_Keywords	Cell division	23	3.9	2.1E–4
GOTerm_BP_FAT	Cell division	23	3.5	9.8E–4
GOTerm_CC_FAT	Microtubule cytoskeleton	32	2.6	3.7E–3
SP_PIR_Keywords	Cell cycle control	8	11.4	6.4E–3

*FDR, False discovery rate adjusted *p* value.

cell cycle occurred compared with 24 h of treatment (Fig. 4). A similar result was observed for Ag^+-treated cells although there were slight differences in the number of genes between Ag^+ and AgNP exposure with more genes upregulated in AgNP-treated cells (Fig. 4). To further investigate the effect of AgNP exposure, synchronized A549 cells were exposed to the same concentrations of Ag^+ or AgNPs as used for the microarray analysis. The cell cycle was investigated after 24-h and 48-h exposure by staining with DAPI and subsequent analysis by flow cytometry. Although treatment with Ag^+ had no effect on the cell cycle compared with the control, exposure to AgNPs significantly increased the amount of cells in the S and G2/M phases (Fig. 5B). In addition, the amount of cells in the S and G2/M phases of the cell cycle increased in a dose dependent manner (Figs. 5A and C). It should be noted that the amount of cells in the G2/M phase did not further increase and that the amount of cells in the S phase went back to the level of the control when investigating the cell cycle after 48 h of exposure with AgNPs (Fig. 5D). In accordance with these investigations, microscopic analysis of synchronized cells revealed a noticeable decrease of dividing cells (Fig. 6).

Regulation of Stress Genes and Production of ROS

Treatment with 1.3 µg/ml Ag^+ or 12.1 µg/ml AgNP (same concentrations as for the microarray) significantly increased the production of ROS in A549 cells (Fig. 7). This is in accordance with the upregulation of a high number of genes related to cellular stress like the heat shock protein superfamily and genes of the metallothionein family (see Supplementary tables 2 and 3). However, validating the effect of Ag^+ and AgNP treatment on the gene expression level of *metallothionein 1B* (*MT1B*) with RT-qPCR showed that exposure to AgNP induced the expression to *MT1B* to a higher degree than Ag^+-treated cells (1.9-fold when comparing cells treated with 1.33 µg/ml Ag^+ with cells exposed to 1.33 µg/ml AgNP; 82-fold when comparing cells treated with 1.33 µg/ml Ag^+ with cells exposed to 12.1 µg/ml AgNP as used for the microarray studies) (Figs. 5E and F). This suggests that AgNPs induce a stronger stress response due to their particular form than the same amount of silver in ionic form.

DISCUSSION

The toxicity of AgNPs has been demonstrated both in *in vitro* and *in vivo* investigations (Bilberg *et al.*, 2011; Foldbjerg *et al.*, 2011, 2009; Kawata *et al.*, 2009). However, it is not entirely clear whether the observed toxicity is due to Ag^+ released from the AgNPs or whether it is related to the AgNP as the concentration of Ag^+ is often not well controlled (Beer *et al.*, 2012). AgNP suspensions can contain up to 69% initial silver ion fraction (Beer *et al.*, 2012), and depending on temperature and the used stabilizing agent, AgNPs dissolve over time (Kittler *et al.*, 2010). The biggest challenge for investigating the toxicity of AgNPs is, therefore, to distinguish the toxicity of AgNPs from that of Ag^+. Accordingly, we compared Ag^+ with AgNPs at concentrations not only representing the initial Ag^+ fraction of the AgNP suspension, as it would be present in the supernatant of the AgNPs at time point zero, but also considering the maximum release of Ag^+ from the AgNPs during exposure based on the dissociation kinetic determined by Kittler *et al.* (2010). The calculated and used Ag^+ concentration of 1.3 µg/ml for treatment of A549 cells corresponds to EC10 for Ag^+ as previously determined by MTT assay (Foldbjerg *et al.*, 2011). To further evaluate the mechanism of toxicity, the effect of

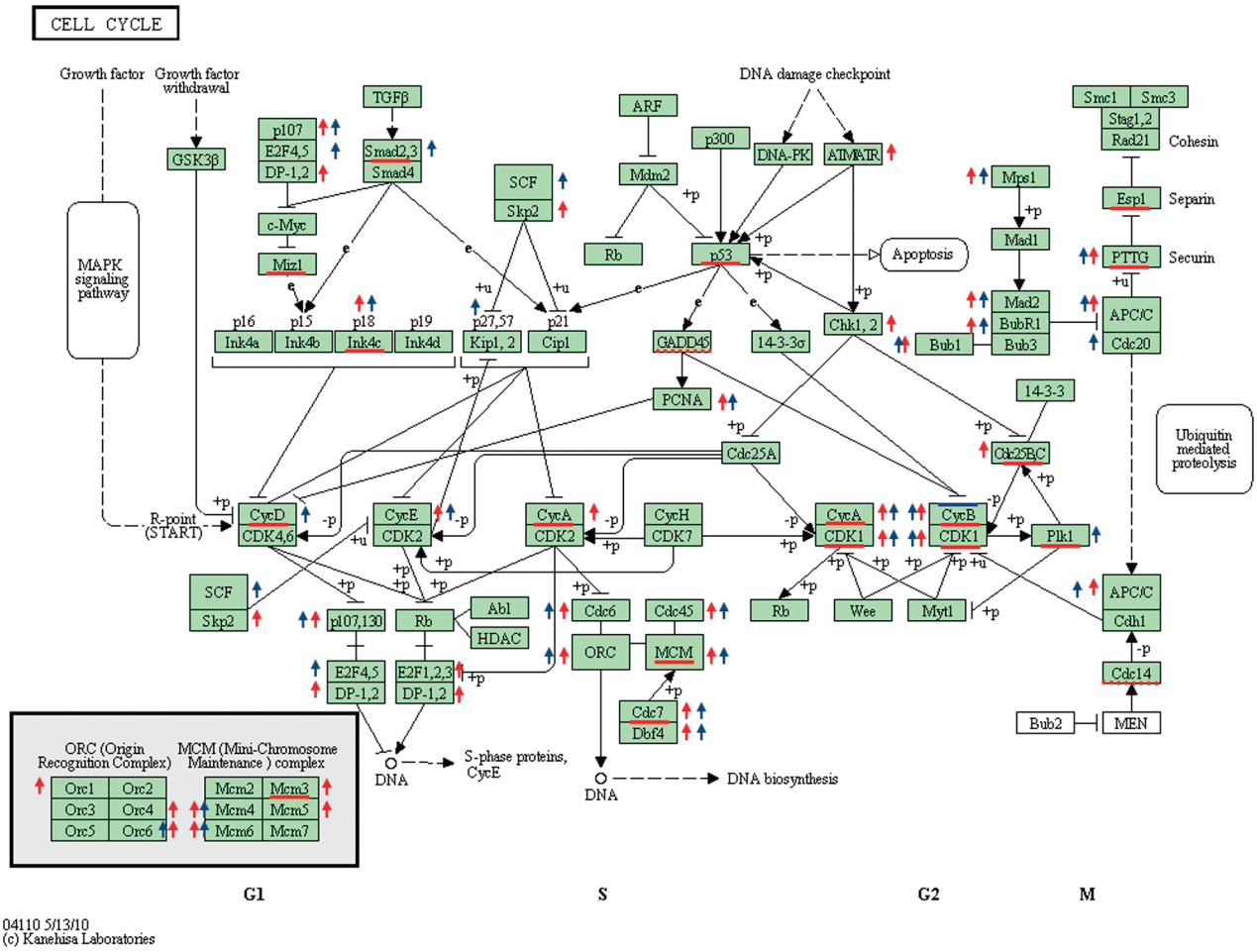

FIG. 4. Cell cycle pathway (KEGG). Red underlined—Genes downregulated in response to 24-h exposure with AgNPs; Red dashed underlined—Genes upregulated in response to 24-h exposure with AgNPs; Red arrow—Genes upregulated in response to 48-h exposure with AgNPs; Blue arrow—Genes upregulated in response to 48-h exposure with Ag^+. Underlined genes without an arrow represent genes with constantly regulated gene expression after 48-h exposure.

AgNPs on the expression of genes was investigated in A549 cells at a relatively low toxicity concentration (EC20) to avoid that cellular processes in necrotic or apoptotic cells degrade the mRNAs, which would ultimately affect the microarray analysis and consequently lead to a misinterpretation of the data. Only a very few investigations have been published concerning the *in vivo* situation of AgNP exposure like, e.g., exposure of workers who manufacture AgNPs. Lee *et al.* (2012) published that two workers in a silver nanomaterial–producing company had a blood Ag concentration of 0.034 and 0.0135 mg/dl Ag and a urinary concentration of 0.043 mg/dl or an undetected Ag level with no health effect in either worker. The used dose of 12.1 µg/ml used in this study is much higher than the reported concentrations in blood and urine. However, we chose this dose to be able to investigate the mechanisms of an acute toxic situation after exposure to AgNPs.

The microarray analysis showed that the number of regulated genes was considerably lower when cells were exposed to Ag^+ compared with exposure to AgNPs. One simple explanation is that the Ag^+ concentration used to simulate the amount of free Ag^+ in the AgNP suspension corresponds to EC10, whereas AgNPs were added at a concentration of 12.1 µg/ml corresponding to EC20. However, when validating some of the differentially regulated genes like *CCNB1*, *HIST1H1B,* and *MT1B* by RT-qPCR, a significant difference between Ag^+-treated cells and AgNP-treated cells could be shown although the same amount of total silver was added. This may be explained by the so-called Trojan horse theory. The plasma membrane functions to some degree as a natural barrier for metal ions, thereby protecting the cells from damage. However, NPs circumvent this barrier when they are taken up by the cells via endocytic pathways, leading to the release of metal ions within the cells as a result of lysosome rupture (Brunner *et al.*, 2006; Studer *et al.*, 2010). In addition, this results in the observed toxicity by generating free radicals within the cells (Karlsson *et al.*, 2009; Midander *et al.*, 2009).

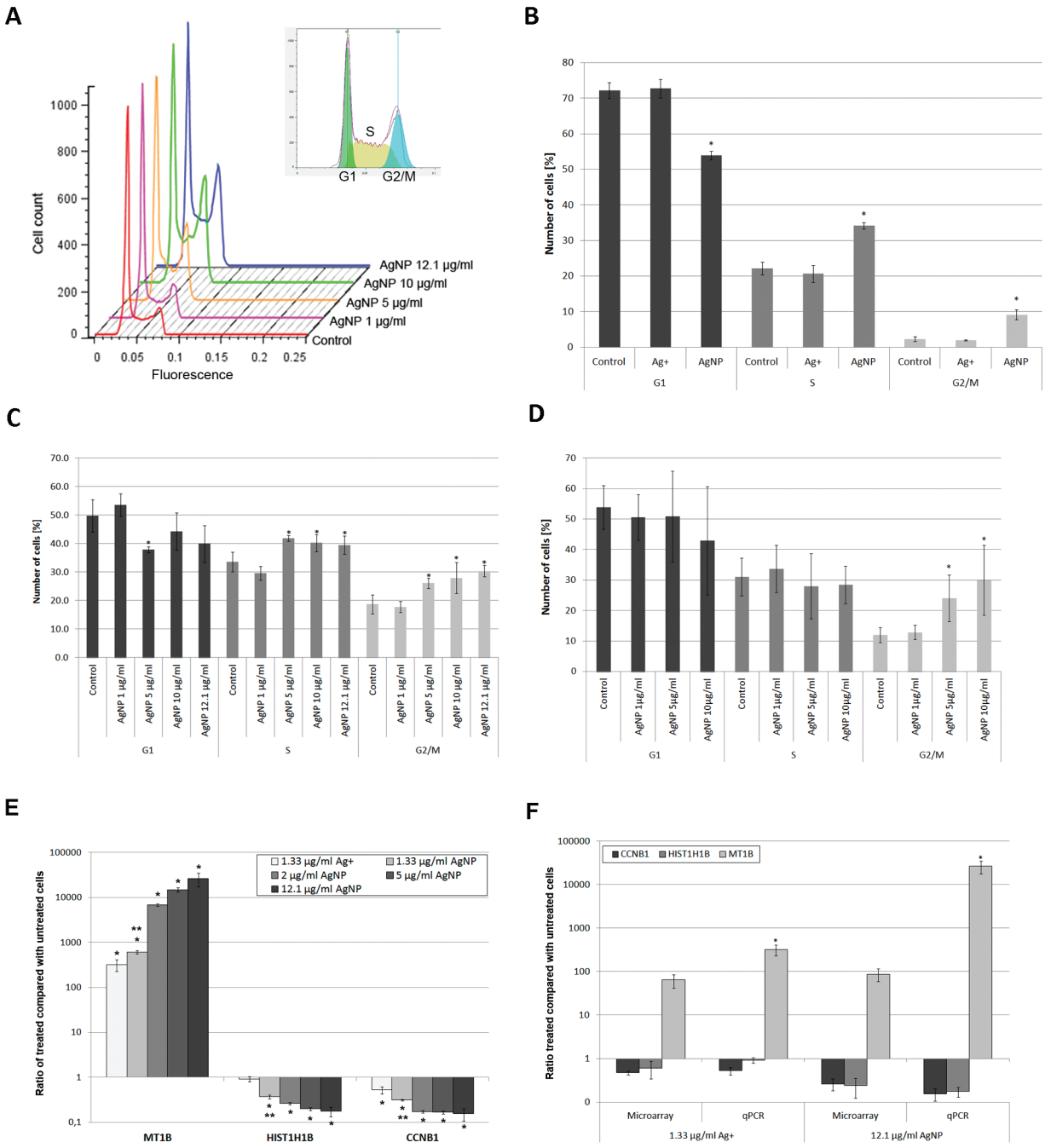

FIG. 5. Cell cycle analysis of cells treated with Ag^+ or AgNPs. Synchronized A549 cells were treated with Ag^+ or AgNPs; the cells were harvested and their DNA stained with DAPI. The DNA content was measured by flow cytometry. (A) Flow cytometry histograms comparing the DNA content of cells treated with different concentrations of AgNPs. (B) Effect of 24-h treatment with 1.3 µg/ml Ag^+, 12.1 µg/ml AgNP compared with control on the cell cycle. (C) Dose-response investigations of the effect of 24-h treatment with AgNPs compared with control. (D) Dose-response investigations of the effect of 48-h treatment with AgNPs compared with control. Data shown in (A)–(D) are expressed as mean ± SD of two independent experiments done in two independent replicas. Statistical significance was calculated by Student's *t*-test and the asterisk depicts $p < 0.05$. (E) Gene regulation of *MT1B*, *HIST1H1B,* and *CCNB1* upon treatment with Ag+ and AgNPs. Data are expressed as mean ± SD of three independent biological replicas done in triplicates. Statistical significance compared with control was calculated by one way ANOVA followed by Tukey's test and * depicts $p < 0.05$. ** depicts $p < 0.05$ for statistical significant difference between 1.33 µg/ml Ag^+ and 1.33 µg/ml AgNPs as calculated by Student's *t*-test. (F) Comparison of gene regulation as measured by microarray and RT-qPCR. Data are expressed as mean ± SD of two independent experiments (microarray) or three independent experiments (RT-qPCR). Statistical significant changes of RT-qPCR data compared with microarray data were analyzed by Student's *t*-test and the asterisk depicts $p < 0.05$.

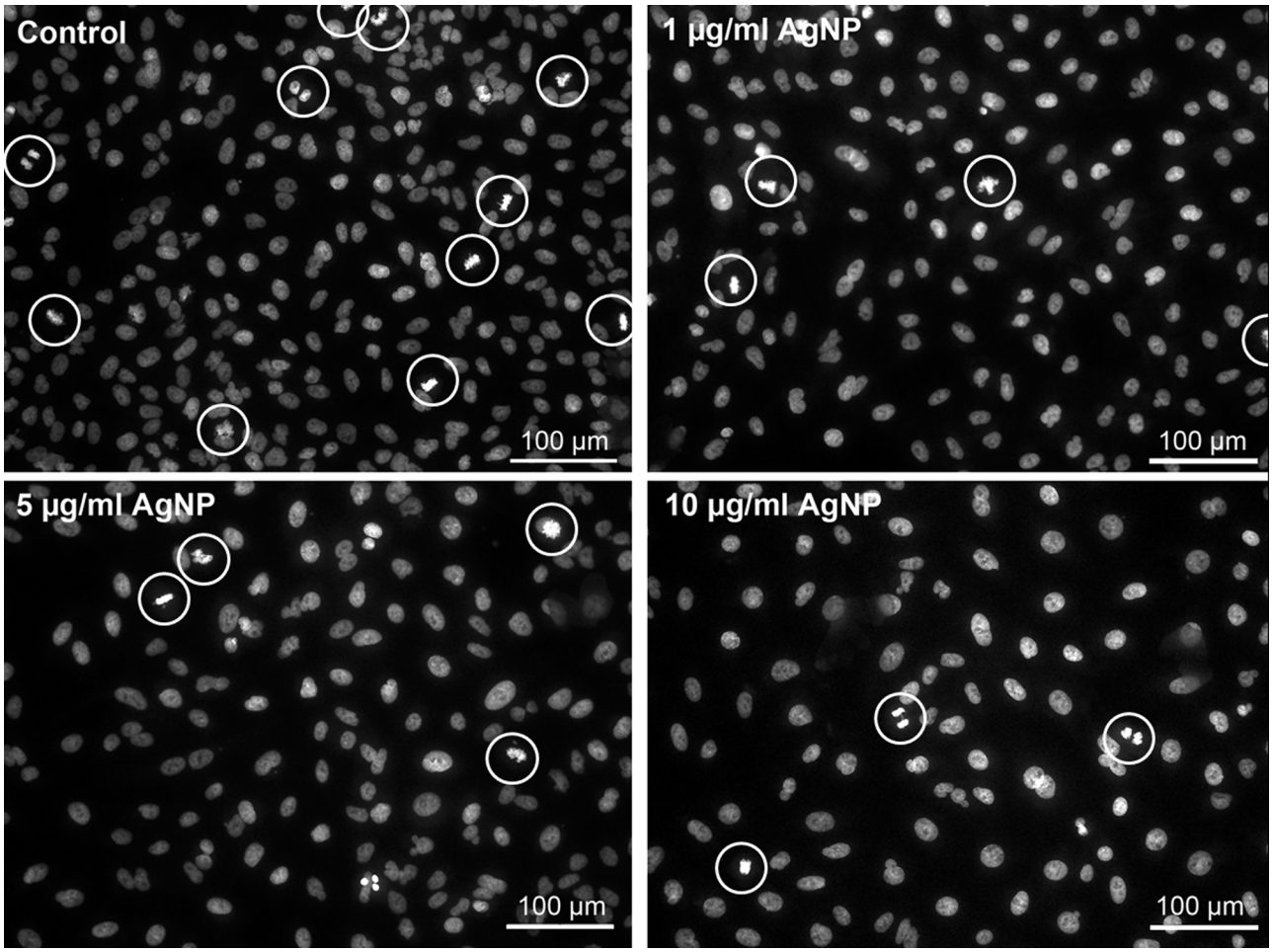

FIG. 6. Microscopy of DNA staining of synchronized A549 cells treated for 24 h with different amounts of AgNPs compared with control. Circles depict dividing cells.

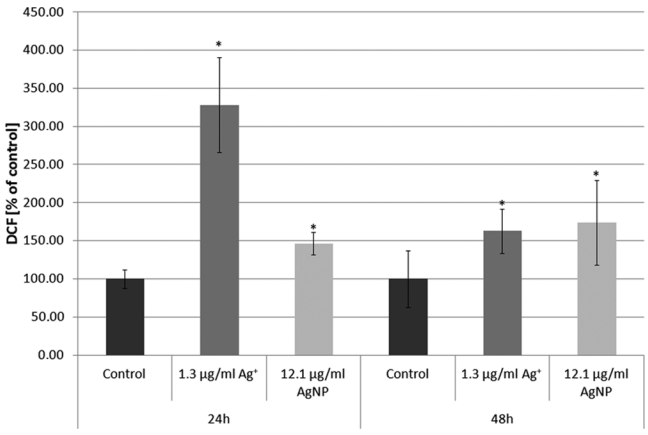

FIG. 7. Investigation of the induction ROS by treatment with Ag^+ and AgNPs. Induction of ROS by treatment with 1.3 µg/ml Ag^+ or 12.1 µg/ml AgNPs compared with control. The increase in DCF fluorescence was measured as a marker for ROS and is presented as percent of control. The data are expressed as mean ± SD of three independent experiments performed in duplicates. The asterisk depicts $p < 0.05$ and statistical significance was calculated by Student's *t*-test.

Strikingly, nearly 80% of all genes induced by Ag^+ were also upregulated in AgNP-treated cells. Bioinformatic analysis of the upregulated genes in response to 24-h exposure with Ag^+ and AgNPs revealed for both similar functional gene groups that were significantly enriched. Noticeably, especially GO terms relating to metal binding and response to metal exposure were significantly enriched. This mainly included genes from the metallothionein superfamily, which could be expected as metals/metal ions are known to induce the expression of these genes (Klaassen *et al*., 2009). Increased expression of metallothionein genes by AgNP is in accordance with the findings of Bouwmeester *et al*. (2011). They investigated the gene expression in the human colon cancer (colorectal adenocarcinoma) Caco2 cells after treatment with AgNPs and Ag^+. We found that a higher number of genes were regulated due to the presence of the AgNPs compared with Ag^+, which is in contrast to the study by Bouwmeester *et al*. (2011). In their study, a significant difference in the gene expression pattern of AgNP-treated cells compared with Ag^+-treated cells was not found. Interestingly, the number of regulated genes upon Ag^+ treatment was

approximately the same in the two studies. However, as they do not use the same array platform, cell line, and AgNP and Ag+ concentrations, a direct comparison of our results is difficult.

Another difference between the studies is the incubation time, as Bouwmeester *et al*. (2011) only treated cells for 4 h with Ag^+ and AgNPs, compared with 24 and 48 h in the study presented here, thus they may only have detected early response genes. The minimum exposure time of 24 h in our study was chosen to cover the time range of all known endocytotic pathways like clathrin-mediated endocytosis and caveolin-mediated endocytosis to ensure that a significant amount of AgNPs were taken up by the cells. Also, the minimum exposure time of 24 h should allow particle interaction with the intracellular compartments, and the effects of these interactions are measured by microarray analysis. The longer exposure time with AgNPs may explain the high number of regulated genes. However, a limitation of exposure for 24 h is that early response genes cannot be detected.

AgNP treatment had an extensive effect on the expression of genes coding for proteins involved in regulation and maintenance of the cell cycle. Noticeable, the vast majority of these regulated genes were downregulated after 24 h of exposure to AgNPs, whereas treatment with Ag^+ had no effect on the cell cycle. It cannot be excluded that AgNPs could directly interact with proteins involved in the cell cycle. Strikingly, the few genes of the cell cycle regulation pathway that were upregulated encode proteins with inhibitory functions, like GADD45, which has been shown to be involved in cell cycle arrest at the G2/M checkpoint by overexpression of *GADD45a* in primary human fibroblasts (Wang *et al*., 1999) and DNA repair (Smith *et al*., 2000). Furthermore, GADD45 has been shown to interact and inhibit the kinase activity of the Cdk1/cyclinB1 complex, which itself plays a key role in the G2/M transition (Vairapandi *et al*., 2002). In addition to the upregulation of *GADD45, Cdk1* and *cyclinB1* were downregulated in response to AgNP treatment. Taken together, our data suggest that 24-h exposure to AgNPs results in cell cycle arrest at the G2/M boundary. But, considering that also other key genes of the cell cycle like cyclin A are downregulated, a general adverse effect on the cell cycle cannot be excluded. After 48 h of exposure to AgNPs, a profound upregulation of genes involved in the maintenance and regulation of cell cycle was observed, and this upregulation was also observed for Ag^+-treated cells although to a lesser extent. The upregulation after 48-h exposure to AgNPs could be an indication of the cells adapting to AgNP exposure. Most of the downregulated genes after 24-h exposure were upregulated after 48 h. However, inhibitor proteins of the cell cycle were still upregulated, e.g., *GADD45*. In addition, a continuous arrest in the G2/M phase of the cell cycle could also be detected by flow cytometry.

Flow cytometric analysis showed an increase of cells in the S and G2/M phases of the cell cycle when cells were treated with AgNP but not when treated with Ag^+. The arrest of cells in the G2/M phase of the cell cycle has previously been reported (Austin *et al*., 2011; Lee YS *et al*., 2011). However, none of these studies reported an accumulation of cells in the S phase. In a very recently published study, we were not able to detect significant changes in the cell cycle of A549 cells exposed to AgNP, which can be explained by the use of nonsynchronized cells in this study (Beer *et al*., 2012). Now, using synchronized cells for the cell cycle investigations, we were able to consistently reproduce the increased number of cells in the S and G2/M phases of the cell cycle. The arrest in the G2/M phase when the cells were treated with AgNPs for 24 h was supported by microscopy studies showing fewer dividing cells compared with the control. However, it should be noted that the amount of cells in the G2/M phase did not further increase after 48 h of treatment and that the amount of cells in the S phase went back to the level of the control. This suggests that there is not a complete arrest in the G2/M phase, but rather a delay of the cell cycle and that the cells are able to overcome this incomplete arrest in the S and G2/M phase as suggested by the microarray data. Taken together, this suggests that AgNPs induce a delay of the cell cycle in the S and G2/M phases and that this delay is specific for AgNPs under the here used experimental conditions (concentration, initial silver ion fraction, and exposure time).

Metallothioneins are not only induced as a response to metal exposure but also by oxidative stress. The cysteines of metallothioneins have been shown to bind oxidant radicals like superoxide and hydroxyl radicals (Formigari *et al*., 2007; Kumari *et al*., 1998). The upregulation of metallothioneins is, therefore, consistent with the induction of ROS by Ag^+ and AgNPs. The induction of ROS by Ag^+ and AgNPs has been shown earlier (Beer *et al*., 2012; Foldbjerg *et al*., 2011; Piao *et al*., 2011). In the present study, an AgNP suspension with a low initial silver ion fraction of 4.99% induced ROS. Interestingly, this induction was much higher for Ag^+ than for AgNPs although the induction of stress response genes including genes encoding heat shock proteins (HSPs) and metallothioneins was higher in AgNP-treated cells. Like metallothioneins, HSPs have been classified as stress response proteins due to their induction by several kinds of cellular stress like infection and inflammation (Santoro, 2000). In the present study, the upregulation of HSP genes included small HSPs, HSP 40, HSP70, HSP90, and HSP110 family. Previously, HSPs have been shown to be induced by several stress conditions that include exposure to heavy metals (Guven and de Pomerai, 1995; Mutwakil *et al*., 1997), where they play a role in maintaining the correct folding of nascent and stress-induced misfolded proteins by preventing protein aggregation or facilitating selective degradation of misfolded or denatured proteins (Gupta *et al*., 2010). The induction of HSPs has previously been associated with oxidative stress (Gorman *et al*., 1999), and recently a correlation between ROS and induction of HSP70 was found in *Drosophila melanogaster* after exposure to AgNPs (Ahamed *et al*., 2010). This is consistent with our microarray results, especially considering that the microarray data reflect gene

expression regulation at the time point of RNA harvest, whereas the ROS data reflect the total amount of ROS present during the exposure period.

In conclusion, although the transcriptional response to exposure with Ag^+ is highly related to the responses caused by exposure to AgNPs, our data suggest that AgNPs, due to their particulate form, affect cells in a more complex way. In addition, our data suggest that the cellular response to Ag^+ is faster and less persisting than for AgNP treatment.

SUPPLEMENTARY DATA

Supplementary data are available online at http://toxsci.oxfordjournals.org/.

FUNDING

Danish Council for Strategic Research funded project "A parallelogram approach to assess the risk of engineered nanotechnology materials" (09-067185).

ACKNOWLEDGMENTS

The authors would like to thank Duy Anh Dang for his excellent technical assistance and Per Guldhammer Henriksen for his help with the AAS measurements. All authors declare not to have any conflicts of interest.

REFERENCES

Ahamed, M., Posgai, R., Gorey, T. J., Nielsen, M., Hussain, S. M., and Rowe, J. J. (2010). Silver nanoparticles induced heat shock protein 70, oxidative stress and apoptosis in *Drosophila melanogaster*. *Toxicol. Appl. Pharmacol.* **242,** 263–269.

Austin, L. A., Kang, B., Yen, C. W., and El-Sayed, M. A. (2011). Nuclear targeted silver nanospheres perturb the cancer cell cycle differently than those of nanogold. *Bioconjug. Chem.* **22,** 2324–2331.

Beer, C., Foldbjerg, R., Hayashi, Y., Sutherland, D. S., and Autrup, H. (2012). Toxicity of silver nanoparticles — Nanoparticle or silver ion? *Toxicol. Lett.* **208,** 286–292.

Bilberg, K., Døving, K. B., Beedholm, K., and Baatrup, E. (2011). Silver nanoparticles disrupt olfaction in Crucian carp (*Carassius carassius*) and Eurasian perch (*Perca fluviatilis*). *Aquat. Toxicol.* **104,** 145–152.

Bouwmeester, H., Poortman, J., Peters, R. J., Wijma, E., Kramer, E., Makama, S., Puspitaninganindita, K., Marvin, H. J., Peijnenburg, A. A., and Hendriksen, P. J. (2011). Characterization of translocation of silver nanoparticles and effects on whole-genome gene expression using an in vitro intestinal epithelium coculture model. *ACS Nano* **5,** 4091–4103.

Brunner, T. J., Wick, P., Manser, P., Spohn, P., Grass, R. N., Limbach, L. K., Bruinink, A., and Stark, W. J. (2006). In vitro cytotoxicity of oxide nanoparticles: Comparison to asbestos, silica, and the effect of particle solubility. *Environ. Sci. Technol.* **40,** 4374–4381.

Drake, P. L., and Hazelwood, K. J. (2005). Exposure-related health effects of silver and silver compounds: A review. *Ann. Occup. Hyg.* **49,** 575–585.

Foldbjerg, R., Dang, D. A., and Autrup, H. (2011). Cytotoxicity and genotoxicity of silver nanoparticles in the human lung cancer cell line, A549. *Arch. Toxicol.* **85,** 743–750.

Foldbjerg, R., Olesen, P., Hougaard, M., Dang, D. A., Hoffmann, H. J., and Autrup, H. (2009). PVP-coated silver nanoparticles and silver ions induce reactive oxygen species, apoptosis and necrosis in THP-1 monocytes. *Toxicol. Lett.* **190,** 156–162.

Formigari, A., Irato, P., and Santon, A. (2007). Zinc, antioxidant systems and metallothionein in metal mediated-apoptosis: Biochemical and cytochemical aspects. *Comp. Biochem. Physiol. C Toxicol. Pharmacol.* **146,** 443–459.

Gorman, A. M., Heavey, B., Creagh, E., Cotter, T. G., and Samali, A. (1999). Antioxidant-mediated inhibition of the heat shock response leads to apoptosis. *FEBS Lett.* **445,** 98–102.

Gupta, S. C., Sharma, A., Mishra, M., Mishra, R. K., and Chowdhuri, D. K. (2010). Heat shock proteins in toxicology: How close and how far? *Life Sci.* **86,** 377–384.

Guven, K., and De Pomerai, D. I. (1995). Differential expression of HSP70 proteins in response to heat and cadmium in *Caenorhabditis elegans*. *J. Therm. Biol.* **20,** 355–363.

Heckmann, L. H., Sørensen, P. B., Krogh, P. H., and Sørensen, J. G. (2011). NORMA-Gene: A simple and robust method for qPCR normalization based on target gene data. *BMC Bioinformatics* **12,** 250.

Hsiao, I. L., and Huang, Y. J. (2011). Effects of various physicochemical characteristics on the toxicities of ZnO and TiO nanoparticles toward human lung epithelial cells. *Sci. Total Environ.* **409,** 1219–1228.

Huang, D. W., Sherman, B. T., and Lempicki, R. A. (2009a). Bioinformatics enrichment tools: Paths toward the comprehensive functional analysis of large gene lists. *Nucleic Acids Res.* **37,** 1–13.

Huang, D. W., Sherman, B. T., and Lempicki, R. A. (2009b). Systematic and integrative analysis of large gene lists using DAVID bioinformatics resources. *Nat. Protoc.* **4,** 44–57.

Karlsson, H. L., Gustafsson, J., Cronholm, P., and Möller, L. (2009). Size-dependent toxicity of metal oxide particles—A comparison between nano- and micrometer size. *Toxicol. Lett.* **188,** 112–118.

Kawata, K., Osawa, M., and Okabe, S. (2009). In vitro toxicity of silver nanoparticles at noncytotoxic doses to HepG2 human hepatoma cells. *Environ. Sci. Technol.* **43,** 6046–6051.

Kittler, S., Greulich, C., Diendorf, J., Köller, M., and Epple, M. (2010). Toxicity of silver nanoparticles increases during storage because of slow dissolution under release of silver ions. *Chem. Mater.* **22,** 4548–4554.

Klaassen, C. D., Liu, J., and Diwan, B. A. (2009). Metallothionein protection of cadmium toxicity. *Toxicol. Appl. Pharmacol.* **238,** 215–220.

Krejsa, C. M., and Schieven, G. L. (2000). Detection of oxidative stress in lymphocytes using dichlorodihydrofluorescein diacetate. *Methods Mol. Biol.* **99,** 35–47.

Kumari, M. V., Hiramatsu, M., and Ebadi, M. (1998). Free radical scavenging actions of metallothionein isoforms I and II. *Free Radic. Res.* **29,** 93–101.

Landsiedel, R., Ma-Hock, L., Kroll, A., Hahn, D., Schnekenburger, J., Wiench, K., and Wohlleben, W. (2010). Testing metal-oxide nanomaterials for human safety. *Adv. Mater. Weinheim* **22,** 2601–2627.

Lee, J. H., Mun, J., Park, J. D., and Yu, I. J. (2012). A health surveillance case study on workers who manufacture silver nanomaterials. *Nanotoxicology* **6,** 667–669.

Lee, Y. S., Kim, D. W., Lee, Y. H., Oh, J. H., Yoon, S., Choi, M. S., Lee, S. K., Kim, J. W., Lee, K., and Song, C. W. (2011). Silver nanoparticles induce apoptosis and G2/M arrest via PKCζ-dependent signaling in A549 lung cells. *Arch. Toxicol.* **85,** 1529–1540.

Marambio-Jones, C., and Hoek, E. M. V. (2010). A review of the antibacterial effects of silver nanomaterials and potential implications for human health and the environment. *J. Nanopart. Res.* **12,** 1531–1551.

Maynard, A. D., Warheit, D. B., and Philbert, M. A. (2011). The new toxicology of sophisticated materials: Nanotoxicology and beyond. *Toxicol. Sci.* **120**(Suppl. 1), S109–S129.

Midander, K., Cronholm, P., Karlsson, H. L., Elihn, K., Möller, L., Leygraf, C., and Wallinder, I. O. (2009). Surface characteristics, copper release, and toxicity of nano- and micrometer-sized copper and copper(II) oxide particles: A cross-disciplinary study. *Small* **5,** 389–399.

Mutwakil, M. H., Reader, J. P., Holdich, D. M., Smithurst, P. R., Candido, E. P. M., Jones, D., Stringham, E. G., and de Pomerai, D. I. (1997). Use of stress-inducible transgenic nematodes as biomarkers of heavy metal pollution in water samples from an English river system. *Arch. Environ. Contam. Toxicol.* **32,** 146–153.

Napierska, D., Thomassen, L. C., Rabolli, V., Lison, D., Gonzalez, L., Kirsch-Volders, M., Martens, J. A., and Hoet, P. H. (2009). Size-dependent cytotoxicity of monodisperse silica nanoparticles in human endothelial cells. *Small* **5,** 846–853.

Oberdörster, G., Oberdörster, E., and Oberdörster, J. (2005). Nanotoxicology: An emerging discipline evolving from studies of ultrafine particles. *Environ. Health Perspect.* **113,** 823–839.

Peirson, S. N., Butler, J. N., and Foster, R. G. (2003). Experimental validation of novel and conventional approaches to quantitative real-time PCR data analysis. *Nucleic Acids Res.* **31,** e73.

Pfaffl, M. W. (2001). A new mathematical model for relative quantification in real-time RT-PCR. *Nucleic Acids Res.* **29,** e45.

Piao, M. J., Kang, K. A., Lee, I. K., Kim, H. S., Kim, S., Choi, J. Y., Choi, J., and Hyun, J. W. (2011). Silver nanoparticles induce oxidative cell damage in human liver cells through inhibition of reduced glutathione and induction of mitochondria-involved apoptosis. *Toxicol. Lett.* **201,** 92–100.

Santoro, M. G. (2000). Heat shock factors and the control of the stress response. *Biochem. Pharmacol.* **59,** 55–63.

Smith, M. L., Ford, J. M., Hollander, M. C., Bortnick, R. A., Amundson, S. A., Seo, Y. R., Deng, C. X., Hanawalt, P. C., and Fornace, A. J., Jr. (2000). p53-mediated DNA repair responses to UV radiation: Studies of mouse cells lacking p53, p21, and/or gadd45 genes. *Mol. Cell. Biol.* **20,** 3705–3714.

Studer, A. M., Limbach, L. K., Van Duc, L., Krumeich, F., Athanassiou, E. K., Gerber, L. C., Moch, H., and Stark, W. J. (2010). Nanoparticle cytotoxicity depends on intracellular solubility: Comparison of stabilized copper metal and degradable copper oxide nanoparticles. *Toxicol. Lett.* **197,** 169–174.

The Woodrow Wilson International Center. The project of emerging nanotechnologies at Woodrow Wilson International Center of Scholars, http://www.nanotechproject.org/inventories/consumer/analysis_draft/. Accessed December 2011.

Vairapandi, M., Balliet, A. G., Hoffman, B., and Liebermann, D. A. (2002). GADD45b and GADD45g are cdc2/cyclinB1 kinase inhibitors with a role in S and G2/M cell cycle checkpoints induced by genotoxic stress. *J. Cell. Physiol.* **192,** 327–338.

van Engeland, M., Ramaekers, F. C., Schutte, B., and Reutelingsperger, C. P. (1996). A novel assay to measure loss of plasma membrane asymmetry during apoptosis of adherent cells in culture. *Cytometry* **24,** 131–139.

Wang, X. W., Zhan, Q., Coursen, J. D., Khan, M. A., Kontny, H. U., Yu, L., Hollander, M. C., O'Connor, P. M., Fornace, A. J., Jr, and Harris, C. C. (1999). GADD45 induction of a G2/M cell cycle checkpoint. *Proc. Natl. Acad. Sci. U.S.A.* **96,** 3706–3711.

Yamamoto, A., Honma, R., Sumita, M., and Hanawa, T. (2004). Cytotoxicity evaluation of ceramic particles of different sizes and shapes. *J. Biomed. Mater. Res. A* **68,** 244–256.